CHAPTER 7

IN VIVO WIRELESS CHANNEL MODELING

A. Fatih Demir, Z. Esat Ankarali, Yang Liu, Qammer H. Abbasi, Khalid Qaraqe, Erchin Serpedin, Huseyin Arslan, and Richard D. Gitlin

7.1 Introduction

Technological advances in biomedical engineering have significantly improved the quality of life and increased the life expectancy of many people. In recent years, there has been increased interest in wireless body area networks (WBANs) research with the goal of satisfying the demand for innovative biomedical technologies and improved healthcare quality [1]-[2]. One component of such advanced technologies is represented by devices such as wireless *in vivo* sensors and actuators, e.g., pacemakers, internal drug delivery devices, nerve stimulators, wireless capsule endoscopes (WCEs), etc. *In vivo* wireless medical devices and their associated technologies represent the next stage of this evolution and offer a cost efficient and scalable solution along with the integration of wearable devices. *In vivo*-WBAN devices (Figure 7.1) are capable of providing continuous health monitoring and reducing the invasiveness of surgery. Furthermore, patient information can be collected over a larger period of time and physicians are able to perform more reliable analysis by exploiting *big data* [3] rather than relying on the data recorded in short hospital visits [4]-[6].

In order to fully exploit and increase further the potential of WBANs for practical applications, it is necessary to accurately assess the propagation of electromagnetic (EM) waveforms in an *in vivo* communication environment (implant-to-implant and implant-to-external device) and obtain accurate channel models that are necessary to optimize the system parameters and build reliable, high-performance communication systems. In particular, creating and accessing such a model is necessary for achieving high data rates, target link budgets,

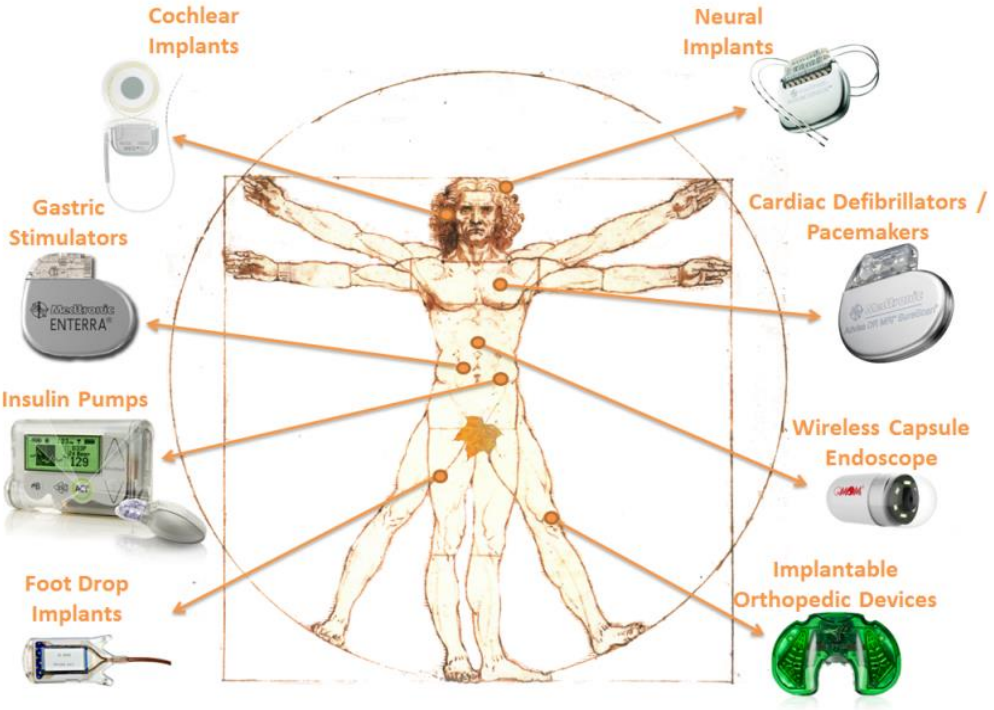

Figure 7.1: *In Vivo*-Wireless Body Area Network.

determining optimal operating frequencies, and designing efficient antennas and transceivers including digital baseband transmitter/receiver algorithms [7]-[8]. Therefore, investigation of the *in vivo* wireless communication channel is crucial to obtain better performance for *in vivo*-WBAN devices. However, research on the *in vivo* wireless communication is still in the early stages and heretofore there have been relatively few studies compared to the on-body wireless communication channel [2], [9]-[11].

The *in vivo* channel exhibits different characteristics than those of the more familiar wireless cellular and Wi-Fi environments since the EM wave propagates through a very lossy environment inside the body and the predominant scatterers are present in the vicinity of the antenna (Figure 7.2). In this chapter, the state-of-the-art of *in vivo* channel characterization is presented and several research challenges are discussed by considering various communication methods, operational frequencies, and antenna designs. Furthermore, a numerical and experimental characterization of the *in vivo* wireless communication channel is described in detail. This chapter aims to provide a more complete picture of this fascinating communications medium and stimulate more research in this important area.

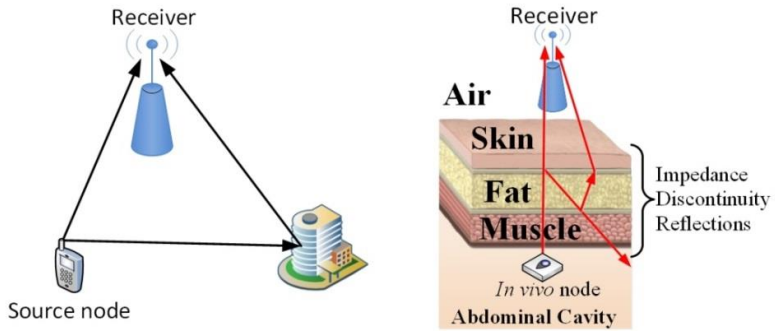

Figure 7.2: The classical communication channel compared with the *in vivo* channel. ©2016 IEEE. Reprinted with permission from [8].

7.2 EM Modeling of the Human Body

In order to investigate the *in vivo* wireless communication channel, accurate body models and knowledge of the electromagnetic properties of the tissues are crucial [2]. Human autopsy materials and animal tissues have been measured over the frequency range 10 Hz to 20 GHz [12] and the frequency dependent dielectric properties of the tissues are modeled using the four-pole Cole-Cole equation, which is expressed as:

$$\varepsilon(\omega) = \varepsilon_{\infty} + \sum_{m=1}^{4} \frac{\Delta\varepsilon_m}{1 + (j\omega\tau_m)^{1-\alpha_m}} + \frac{\sigma_s}{j\omega\varepsilon_0} \qquad (7.1)$$

where ε_{∞} stands for the body material permittivity at terahertz frequency, ε_0 denotes the free-space permittivity, σ_s represents the ionic conductivity and $\Delta\varepsilon_m$, τ_m, α_m are the body material parameters for each anatomical region. The parameters for anatomical regions are provided in [13] and the electromagnetic properties such as conductivity, relative permittivity, loss tangent, and penetration depth can be derived using these parameters in equation (7.1).

Various physical and numerical phantoms have been designed in order to simulate the dielectric properties of the tissues for experimental and numerical investigation [14]. These can be classified as homogeneous, multi-layered and heterogeneous phantom models. Although, heterogeneous models provide a more realistic approximation to the human body, design of physical heterogeneous phantoms is quite difficult and performing numerical experiments on these models is very complex and resource intensive. On the other hand, homogeneous or multi-

layer models cannot differentiate the EM wave radiation characteristics for different anatomical regions. Figure 7.3 shows examples of heterogeneous physical and numerical phantoms.

Analytical methods are generally viewed as infeasible and require extreme simplifications. Therefore, numerical methods are used for characterizing the *in vivo* wireless communication channel. Numerical methods provide less complex and appropriate approximations to Maxwe l l èqu ations via various techniques, such as uniform theory of diffraction (UTD), method of moments (MoM), finite element method (FEM) and finite-difference time-domain method (FDTD). Each method has its own pros and cons and should be selected based on the simulation model and size, operational frequency, available computational resources and interested characteristics, such as power delay profile (PDP), specific absorption rate (SAR), etc. A detailed comparison of these methods is available in [2] and [15].

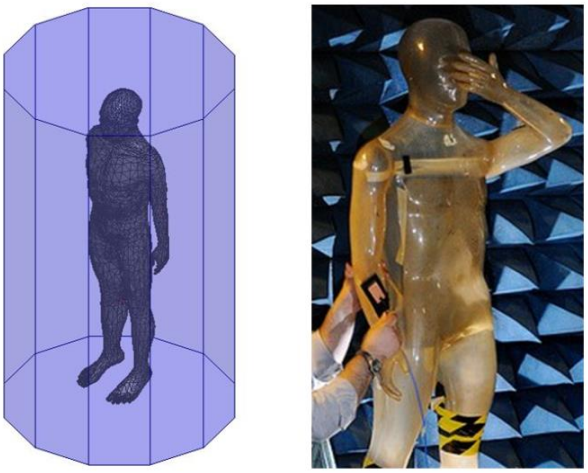

Figure 7.3: Heterogeneous human body models: (a) HFSS® model [19] (b) physical phantom [14]. ©2016 IEEE. Reprinted with permission from [57].

It may be preferable that numerical experiments should be confirmed with real measurements. However, performing experiments on a living human is carefully regulated. Therefore, anesthetized animals [16]-[17] or physical phantoms, allowing repeatability of measurement results, [14], [18] are often used for experimental investigation. In addition, the first such study conducted on a human cadaver was reported in [20].

7.3 EM Wave Propagation through Human Tissues

Propagation in a lossy medium, such as human tissues, results in a high absorption of EM energy [21]. The absorption effect varies with the frequency dependent electrical characteristics of the tissues, which mostly consist of water and ionic content [22]. The specific absorption rate (SAR) provides a metric for the amount of absorbed power in the tissue and is expressed as follows [23]:

$$\text{SAR} = \frac{\sigma E^2}{\rho} \qquad (8)$$

where σ, E and ρ represent the conductivity of the material, the RMS magnitude of the electric field and the mass density of the material, respectively. The Federal Communications Commission (FCC) recommends the SAR to be less than 1.6 W/kg taken over a volume having 1 gram of tissue [24].

When a plane EM wave propagates through the interface of two media having different electrical properties, its energy is partially reflected and the remaining portion is transmitted through the boundary of this media. Superposition of the incident and the reflected wave can cause a standing wave effect that may increase the SAR values [22]. A multilayer tissue model at 403 MHz, where each layer extends to infinity (much larger than the wavelength of EM waves) and the dielectric values are calculated using [25], is illustrated in Figure 7.4. If there is a high contrast in the dielectric values of mediums/tissues, wave reflection at the boundary increases and transmitted power decreases.

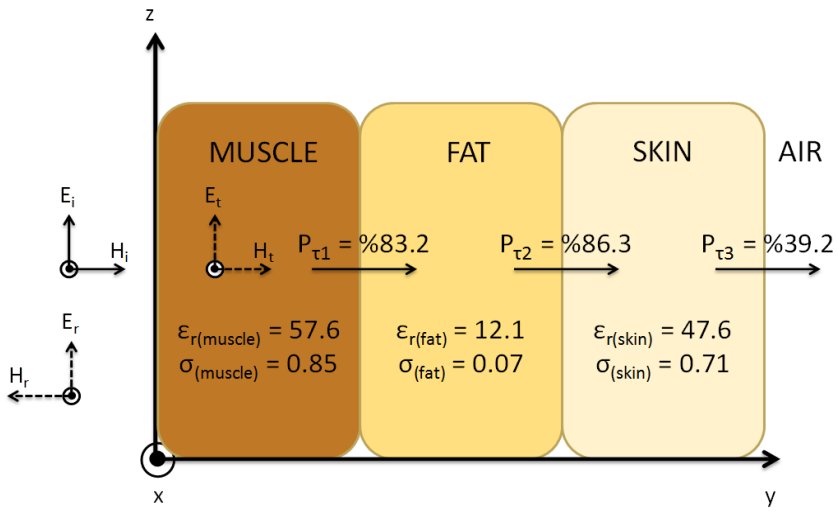

Figure 7.4: Multi-layer human tissue model at 403 MHz (ε: Permittivity, σ Conductivity, P τ Power transmission factor). ©2016 IEEE. Reprinted with permission from [57].

In addition to the absorption and reflection losses, EM waves also suffer from expansion of the wave fronts (which assume an ever-increasing sphere shape from an isotropic source in free space), diffraction and scattering (which depend on the wavelength of EM wave). Section 7.6 discusses *in vivo* propagation models by considering these effects in detail.

7.4 Frequency of Operation

Since EM waves propagate through the frequency dependent materials inside the body, the operating frequency has an important effect on the communication channel. Accordingly, the allocated and recommended frequencies are summarized including their effects for the *in vivo*

Table 7.1: Frequency bands and bandwidths for the three different propagation methods in IEEE 802.15.6. ©2016 IEEE. Reprinted with permission from [57].

Propagation Method	IEEE 802.15.6 Operating Freq. Bands		Selected References
	Frequency Band	BW	
Narrow Band Communications	402 - 405 MHz	300 kHz	[7], [14] , [22], [31] [32], [36], [47]
	420 - 450 MHz	300 kHz	
	863 - 870 MHz	400 kHz	[7], [14], [31], [36], [45], [47]
	902 - 928 MHz	500 kHz	
	950 - 956 MHz	400 kHz	
	2360 - 2400 MHz	1 MHz	[7], [14], [36], [51]
	2400 - 2438.5 MHz	1 MHz	
UWB Communications	3.2 - 4.7 GHz	499 MHz	[17], [28], [36], [51]
	6.2 - 10.3 GHz	499 MHz	
Human - Body Communications	16 MHz	4 MHz	[26], [27]
	27 MHz	4 MHz	

wireless communications channel in this section. The IEEE 802.15.6 standard [1] was released in 2012 to regulate short-range wireless communications inside or in the vicinity of the human body, and are classified as narrow band (NB) communications, ultra-wide band communications (UWB) and human-body communications (HBC) [26], [27]. The frequency bands and channel bandwidths (BW) allocated for these communication methods are summarized in Table 7.1. An IEEE 802.15.6 compliant *in vivo*-WBAN device must operate in at least one of these frequency bands.

NB communications operate at lower frequencies compared to UWB communications and hence suffer less from absorption. This can be appreciated by considering equations (7.1) and (7.2) that describe the absorption as a function of frequency. The medical device radio communications service (MedRadio uses discrete bands within the 401-457 MHz spectrum including the international medical implant communication service (MICS) band) and medical body area network (MBAN, 2360-2400 MHz) are allocated by the FCC for medical devices usage. Therefore, co-user interference problems are less severe in these frequency bands. However, NB communications are only allocated small bandwidths (1 MHz at most) in the standard as shown in Table 7.1. The IEEE 802.15.6 standard does not define a maximum transmit power and the local regulatory bodies limit it. The maximum power is restricted to 25 W EIRP (Equivalent Radiated Isotropic Power) by FCC, whereas it is set to 25 W ERP (Equivalent Radiated Power) by ETSI (European Telecommunication Standards Institute) for the 402-405 MHz band.

UWB communications is a promising technology to deploy inside the body due to its inherent features including high data rate capability, low power, improved penetration (propagation) abilities through tissues and low probability of intercept. The large bandwidths for UWB (499 MHz) enable high data rate communications and applications. Also, UWB signals are inherently robust against detection and smart jamming attacks because of their extremely low maximum effective isotropic radiated power (EIRP) spectral density, which is -41.3 dBm/MHz [28], [29]. On the other hand, UWB communications inside the body suffers from pulse distortion caused by frequency dependent tissue absorption and compact antenna design. Recently, the terahertz frequency band has also been a subject of interest for *in vivo* propagation and it is regarded as one of the most promising bands for the EM paradigm of nano-communications [30].

7.5 *In Vivo* Antenna Design Considerations

Unlike free-space communications, *in vivo* antennas are often considered to be an integral part of the channel and they generally require different specifications than *ex vivo* antennas [2], [31] – [33]. In this section, we will describe their salient differences as compared to the *ex vivo*

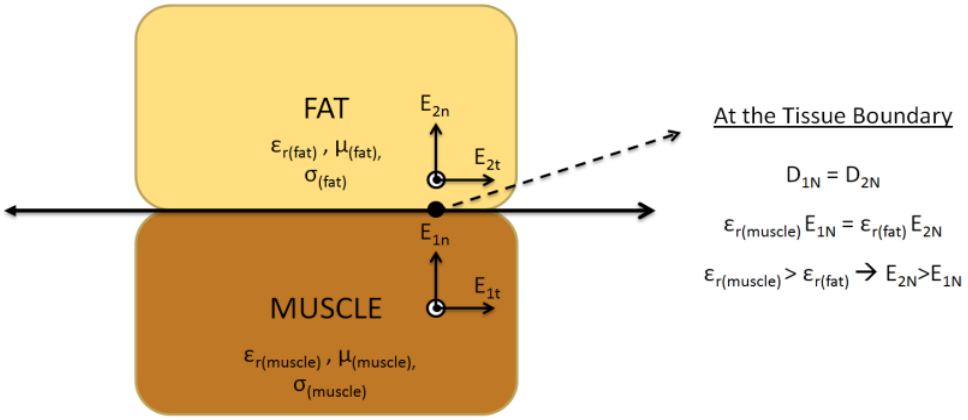

Figure 7.5: EM propagation through tissue interface.

antennas.

In vivo antennas are subject to strict size constraints and in addition need to be bio-compatible. Although, copper antennas have better performance, only specific types of materials such as titanium or platinum should be used for *in vivo* communications due to their noncorrosive chemistry [6]. The standard definition of the gain is not valid for *in vivo* antennas since it includes body effects [34], [35]. As noted above, the gain of the *in vivo* antennas cannot be separated from the body effects as the antennas are considered to be an integral part of the channel. Hence, the *in vivo* antennas should be designed and placed carefully in order not to harm the biological tissues and to provide power efficiency. When the antennas are placed inside the human body, their electrical dimensions and gains decrease due to the high dielectric permittivity and high conductivity of the tissues, respectively [36]. For instance, fat has a lower conductivity than skin and muscle. Therefore, *in vivo* antennas are usually placed in a fat (usually subcutaneous fat -SAT-) layer to increase the antenna gain. This placement is also provides less absorption losses due to shorter propagation path. However, the antenna size becomes larger in this case. In order to reduce high losses inside the tissues, a high permittivity, low loss coating layer can be used. As the coating thickness increases, the antenna becomes less sensitive to the surrounding material [36]-[37].

Lossy materials covering the *in vivo* antenna change the electrical current distribution in the antenna and radiation pattern [18]. It is reported in [31] that directivity of *in vivo* antennas increases due to the curvature of body surface, losses and dielectric loading from the human body. Therefore, this increased directivity should be taken into account as well in order not to harm the tissues in the vicinity of the antenna [23].

In vivo antennas can be classified into two main groups as electrical and magnetic antennas. Electrical antennas, e.g., dipole antennas, generate electric fields (E-field) normal to the tissues, while magnetic antennas, e.g., loop antennas produce E-fields tangential to the human tissues [38]. Normal E-field components at the medium interfaces overheat the tissues due to the boundary condition requirements [39] as illustrated in Figure 7.5. The muscle layer has a larger permittivity value than the fat layer and hence, the E-field increases in the fat layer. Therefore, magnetic antennas allow higher transmission power for *in vivo* WBAN devices as can be

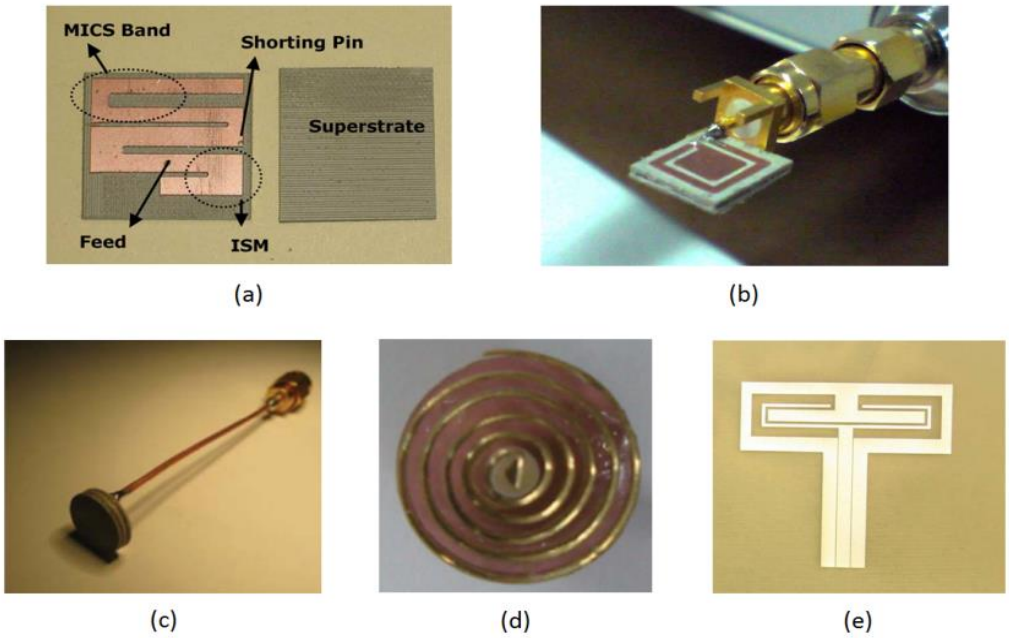

Figure 7.6*:* Selected *in vivo* antenna samples: a) A dual-band implantable antenna [41], b) A miniaturized implantable broadband stacked planar inverted-F antenna (PIFA) [42], c) A miniature scalp-implantable [43], d) A wideband spiral antenna for WCE [16], e) An implantable folded slot dipole antenna [44]. ©2016 IEEE. Reprinted with permission from [57].

appreciated by Eq. 2. In practice, magnetic loop antennas require large sizes, which is a challenge to fit inside the body. Accordingly, smaller size spiral antennas having a similar current distribution as loop antennas can be used for *in vivo* devices [40]. Several selected sample antennas designed for *in vivo* communications are shown in Figure 7.6.

7.6 *In Vivo* EM Wave Propagation Models

The important factors for *in vivo* wireless communication channel characterization, such as EM modeling of the human body, propagation through the tissues, and selection of the operational frequency have been discussed in detail in the preceding sections. Further, the main differences between *in vivo* and *ex vivo* antenna designs were discussed ---principally that the antenna must be considered as an integral part of the *in vivo* channel. In this section, the focus is on EM wave propagation inside the human body considering the anatomical features of organs and tissues. Then, the analytical and statistical path loss models will be presented. Since the EM wave propagates through a very lossy environment inside the body and predominant scatterers are present in the near-field region of the antenna, the *in vivo* channel exhibits different characteristics than those of the more familiar wireless cellular and Wi-Fi environments.

EM wave propagation inside the body is subject-specific and strongly related to the location of the antenna as demonstrated in [7], [18], [20], [31] and [45]. Therefore, channel characterization is generally investigated for a specific part of the human body. Figure 7.7 shows several investigated anatomical regions for various *in vivo*-WBAN applications. For example, the heart area has been studied for implantable cardioverter defibrillators and pacemakers, while the gastrointestinal tract (GI) including esophagus, stomach and intestine has been investigated for

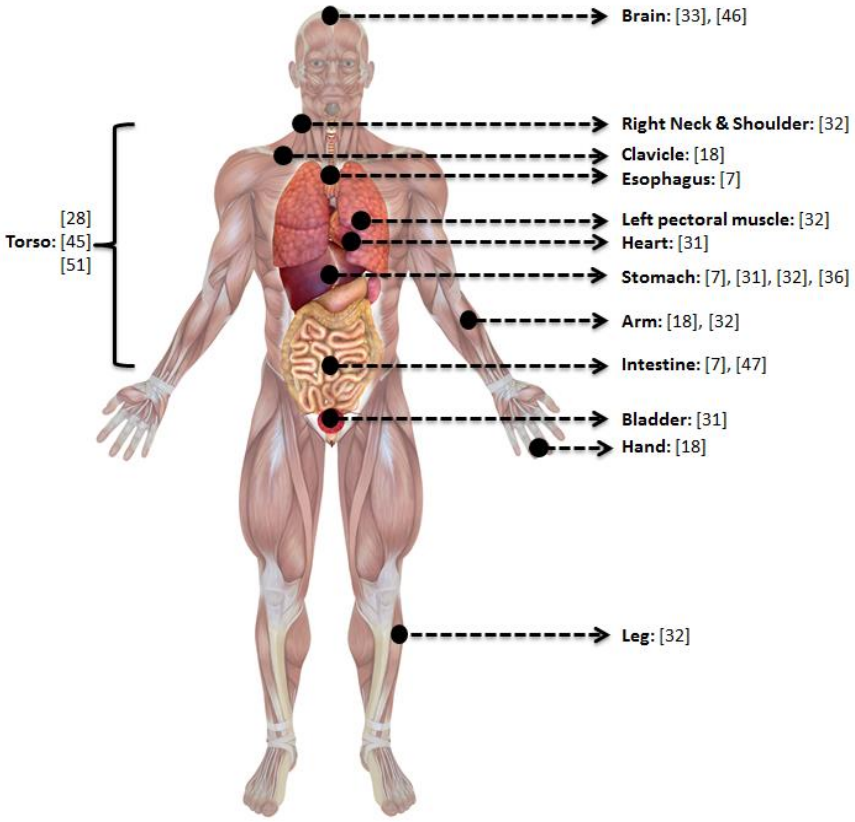

Figure 7.7: Investigated anatomical human body regions.

WCE applications. The bladder region is studied for wirelessly controlled valves in the urinary tract and the brain is investigated for neural implants [33], [46]. Also, clavicle, arm and hands are specifically studied as they are affected less by the *in vivo* medium.

When the *in vivo* antenna is placed in an anatomically complex region, path loss, a measure of average signal power attenuation, increases [7]. This is the case with the intestine which presents a complex structure with repetitive, curvy-shaped, dissimilar tissue layers, while the stomach has a smoother structure. As a result, the path loss is greater in the intestine than in the stomach even at equal *in vivo* antenna depths [7].

Various analytical and statistical path loss formulas have been proposed for the *in vivo* channel in the literature as listed in Table 7.2. These formulas have been derived considering different shadowing phenomena for the *in vivo* medium. The initial three models are functions of the Friis transmission equation [52], return loss and absorption in the tissues. These models are valid, when either the far field conditions are fulfilled or few scattering objects exist between the transmitter and receiver antennas. In the first model, the free space path loss (FSPL) is expressed by the Friis transmission equation. FSPL mainly depends on the gain of antennas, distance and operating frequency. Its dependency on distance is a result of expansion of the wave fronts as explained in Section 7.3. Additionally, FSPL is frequency dependent due to the relationship between the effective area of the receiver antenna and wavelength. The two equations of the FSPL model in Table 7.2 are derived including the antenna return loss and absorption in the tissues. Another analytical model, PMBA [48], calculates the SAR over the entire human body for the far and near fields, and gives the received power using the calculated absorption. Although, these analytical expressions provide intuition about each component of the propagation models, they are not practical for link budget design as was the case with the wireless cellular communication environment.

The channel modeling subgroup (Task Group 15.6), which worked on developing the IEEE 802.15.6 standard, submitted their final report on body area network (BAN) channel models in November 2010. In this report, it is determined that the Friis transmission equation can be used for *in vivo* scenarios by adding a random variation term and the path loss is modeled statistically

Table 7.2: A review of selected studied path loss models for various scenarios.

Model	Formulation
FSPL [31]	$P_r = P_t\, G_t\, G_r \left(\frac{\lambda}{4\pi R}\right)^2$
FSPL with RL [31], [36]	$P_r = P_t\, G_t\, (1 - \lvert S_{11}\rvert^2)\, G_r\, (1 - \lvert S_{22}\rvert^2) \left(\frac{\lambda}{4\pi R}\right)^2$
FSPL with RL and Absorption [40]	$P_r = P_t\, G_t\, (1 - \lvert S_{11}\rvert^2)\, G_r\, (1 - \lvert S_{22}\rvert^2) \left(\frac{\lambda}{4\pi R}\right)^2 (e^{-\alpha R})^2$
PMBA for near and far field [48]	$P_{rn} = \frac{16\boldsymbol{\delta}(P_t - P_{NF})}{\pi L^2} A_e$, $P_{rf} = \left(\frac{(P_t - P_{NF} - P_{FF})\lambda^2}{4\pi R^2}\right) G_t\, G_r$
Statistical Model - A [45], [51]	$PL(d) = PL_0 + n(d/d_0) + S \quad (d_0 \le d)$
Statistical Model - B [14], [31], [32]	$PL(d) = PL(d_0) + 10n\log_{10}(d/d_0) + S \quad (d_0 \le d)$

P_r/P_t stands for the received/transmitted power; G_r/G_t denotes the gain of the receiver/transmitter antenna; ∂ represents the free space wavelength; R is the distance between transmitter and receiver antennas, |S11| and |S22|stand for the reflection coefficient of receiver/transmitter antennas; ώis the attenuation constant, P_{NF} /P_{FF} is the loss in the near/far fields; ŭis A_e/A where A_e is the effective aperture and A is the physical aperture of the antenna; L is the largest dimension of the antenna; d is the depth distance from the body surface, d_0 is the reference depth distance, n is the path loss exponent; PL_0 is the intersection term in dB; S denotes the random shadowing term. Abbreviations: FSPL represents the free space path loss in the far field, RL is the return loss, and PMBA denotes the propagation loss model.

with a log-normal distributed random shadowing *S* and path loss exponent *n* [49], [50]. The path loss exponent (*n*) heavily depends on environment and is obtained by performing extensive simulations and measurements. In addition, the shadowing term (*S*) depends on the different body materials (e.g. bone, muscle, fat, etc.) and the antenna gain in different directions [32]. The research efforts on assessing the statistical properties of the *in vivo* propagation channel have not finalized. There are still many open research efforts dedicated to building analytical models for different body parts and operational frequencies [14], [20], [31], [32], [45], [51].

7.7 *In Vivo* Channel Characterization

The numerical *in vivo* channel characterization was performed in [45] using ANSYS HFSS® 15.0, which is a full wave electromagnetic field simulator based on the Finite Element Method (FEM). ANSYS also provides a detailed human body model of adult male. The numerical investigation was validated by conducting experiments on a human cadaver in a laboratory environment [20]. Istanbul Medipol University provided the ethical approval for the study and medical assistance for this study.

7.7.1 Simulation Setup

The simulations [45] have been designed based on an implant to external device (in-body to on-body) communications scenario. The human male torso area was divided into four subregions considering the major internal organs: heart, stomach, kidneys and intestine as shown in Figure 7.8. The measurements were performed in each subregion by rotating both the receiver (*ex vivo*) and transmitter antennas (*in vivo*) around the body on a plane at 22.5° angle increments as shown in Figure 7.9. For each location of the *ex vivo* antenna (5 cm away from the body surface), the *in vivo* antenna was placed at 10 different depths (10 mm to 100 mm). Moreover, the antennas were placed in the same direction in order to prevent polarization losses.

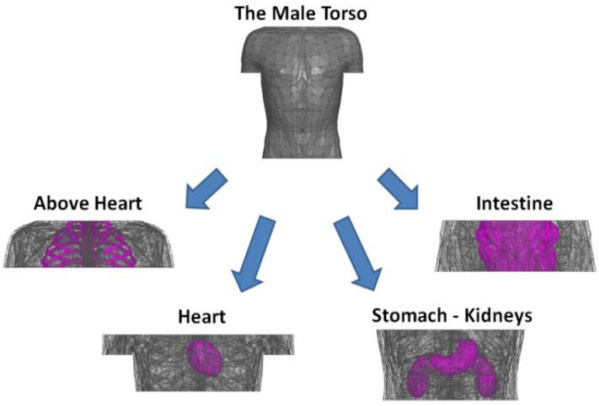

Figure 7.8: Investigated anatomical human body regions. ©2014 IEEE. Reprinted with permission from [45].

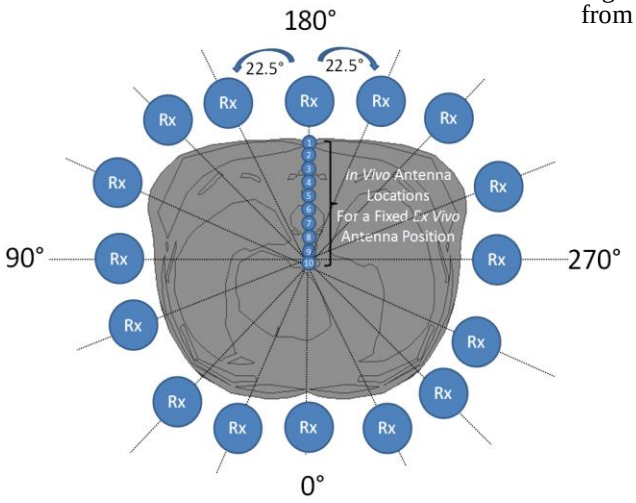

Figure 7.9: *In vivo* and *ex vivo* antenna locations in the simulation. 16 (angles) x 10 (depth) x 4(regions) = 640 simulations are performed for path loss in total. ©2014 IEEE. Reprinted with permission from [45].

Omni-directional dipole antennas at 915 MHz were deployed in simulations for simplicity. The dipole antenna size is proportional to the wavelength, which changes with respect to both frequency and permittivity. Although, the frequency of operation was fixed in this study, the permittivity of the environment was variable. Therefore, the antennas were optimized inside the body with respect to the average torso permittivity in order to obtain maximum power delivery. In addition, a few antenna locations with high return loss (i.e., >-7dB) discarded from the data.

7.7.2 Experimental Setup

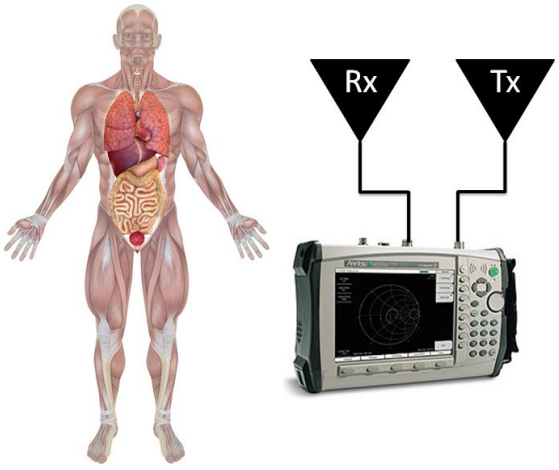

Figure 7.10: Experiment setup for *in vivo* channel. ©2015 IEEE. Reprinted with permission from [20].

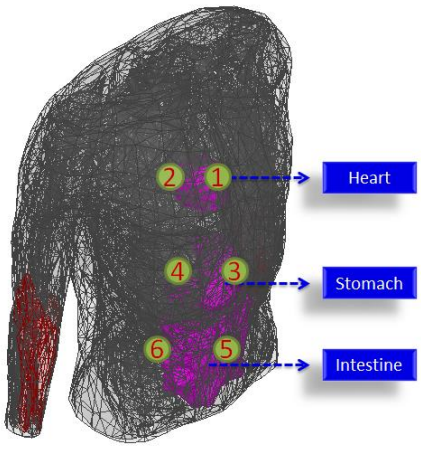

Figure 7.11: Measurement locations on human cadaver. ©2015 IEEE. Reprinted with permission from [20].

In order to validate our simulation results in [45], we conducted experiments on a human cadaver with a similar setup [20]. The human male torso area was investigated at 915 MHz by measuring the channel response through a vector network analyzer (VNA), while using two antennas, one (*in vivo*) [53], and other a dipole antenna (*ex vivo*) as illustrated in Figure 7.10. The *in vivo* antenna was placed at six different locations (Figure 7.11) inside the body around heart, stomach and intestine by a physician. The antennas were located in the same orientation and all return loss values were less than -7dB in the experiment dataset.

7.7.3 Results

7.7.3.1 Location Dependent Characteristics

The location dependent characteristics of the *in vivo* path loss have investigated at 915 MHz. The EM signal propagates through different organs and tissues for various antenna locations that the path loss varies significantly even for equal *in vivo* depths. Figure 7.12 presents the mean path loss for each angular position (see Figure 7.9). It is observed that 0^o has the highest path loss, whereas symmetric locations, 112.5^o and 247.5^o have the lowest attenuation. In addition, the number of scattering objects (random variables) increases as the *in vivo* antenna is placed deeper and the variance of path loss increases as well due to summation of random variables.

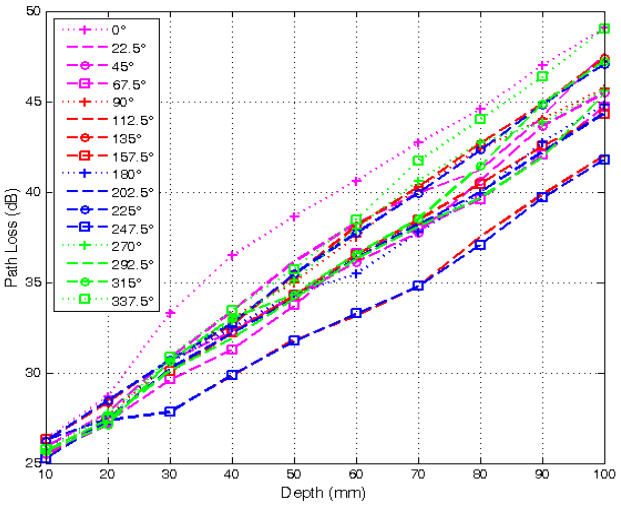

Figure 7.12: Path loss vs *in vivo* depth at 915 MHz ©2014 IEEE. Reprinted with permission from [45].

Figure 7.13 shows the scatter plot of path loss versus depth and the *in vivo* path loss is modeled statistically as a function of depth

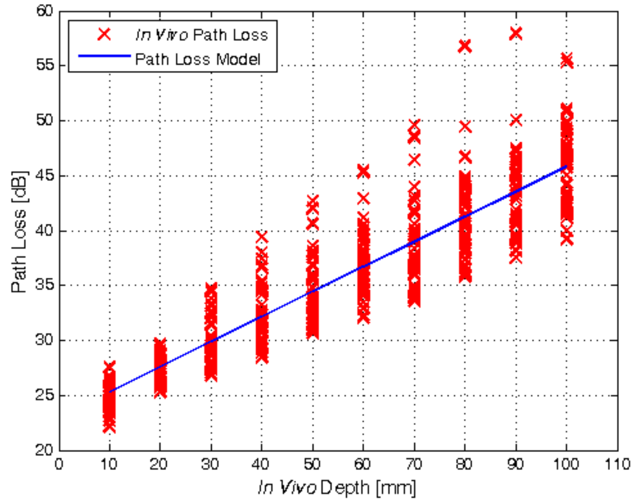

Figure 7.13: Path loss vs *in vivo* depth at 915 MHz.
©2014 IEEE. Reprinted with permission from [45].

by the following equation in dB:

$$PL(d) = PL_0 + 10\,m\,\log_{10}(d/d_0) + S, \quad d \geq d_0$$

where d is the depth distance from the body surface in millimeters, d_0 stands for the reference depth distance (i.e. 10mm), PL_0 represents the intersection term in dB, m denotes the decay rate of received power and S is the shadowing term in dB, which is a normally distributed random variable with zero mean and variance σ^2. The parameters for the statistical *in vivo* path loss model are provided in Tables 7.3 and 7.4. There exists a 30% difference between the received power decay rates (m) of heart and stomach areas. In addition, the path loss at heart and intestine areas exhibit more deviation around the mean than other two regions. It could be concluded that the path loss increases significantly, when the *in vivo* antenna is placed in an anatomically complex region as also reported in [7].

The numerical studies were validated with experiments on a human cadaver at 915 MHz. The *in vivo* antennas were placed at six different locations as shown in Figure 7.11 and the *ex vivo* antenna was placed 2 cm away from the body surface. Table 7.5 presents the path loss values for the selected *in vivo* locations and a comparison of experimental results with numerical studies are provided in Figure 7.14. The discrepancies should have occurred due to additional losses which are not considered in simulations.

The angular dependent characteristics of the *in vivo* channel were investigated by performing further simulations at 0.4 GHz, 1.4 GHz and 2.4 GHz. The *in vivo* antenna was fixed inside the

Table 7.3: Parameters for the statistical path loss model (Body Region). ©2014 IEEE. Reprinted with permission from [45].

Body Area \ Parameters	PL_0[dB]	m	σ
Above Heart	24.75	2.30	3.73
Heart	22.70	1.96	2.38
Stomach - Kidneys	22.56	2.55	1.79
Intestine	24.23	2.31	3.47
Overall Torso Area	23.56	2.28	3.38

Table 7.4: Parameters for the statistical path loss model (Body Side). ©2014 IEEE. Reprinted with permission from [45].

Body Area \ Parameters	PL_0[dB]	m	σ
Anterior	23.83	2.46	3.51
Posterior	23.76	2.21	1.92
Left Lateral	23.34	2.28	3.67
Right Lateral	23.22	2.27	3.51
Overall Torso Area	23.56	2.28	3.38

Table 7.5: Path loss values for selected *in vivo* locations. ©2015 IEEE. Reprinted with permission from [20].

Location	*In Vivo* Depth	Path Loss
01) Above Heart	3 cm	45.32 dB
02) Below Heart	8 cm	55.61 dB
03) Above Stomach	5 cm	48.19 dB
04) Inside Stomach	9 cm	50.80 dB
05) Above Intestine	2 cm	29.95 dB
06) Below Intestine	10 cm	50.47 dB

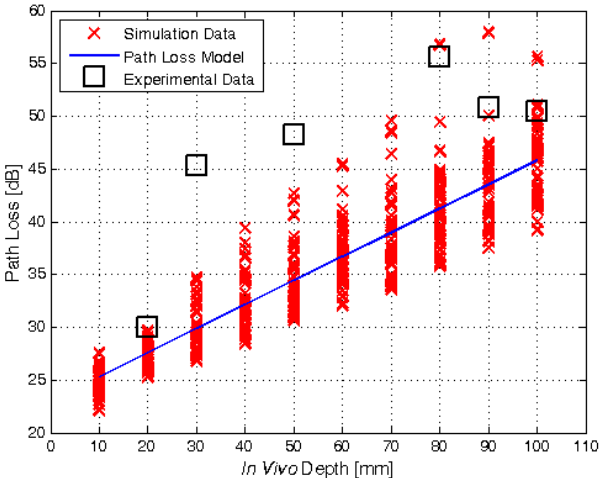

Figure 7.14: Path loss versus *in vivo* depth from body surface. ©2015 IEEE. Reprinted with permission from [20].

abdomen (78mm in depth from body surface) and the *ex vivo* antenna was rotated on the body surface with the azimuth angle of π ϳϭσ υ ϖwith υ ϊincrement. The results are presented in Figure 7.15 and Table 7.6. It could be observed that the angular dependency (i.e. the variation of the path loss vs. azimuth angle) in terms of peak to average ratio is similar for different frequencies.

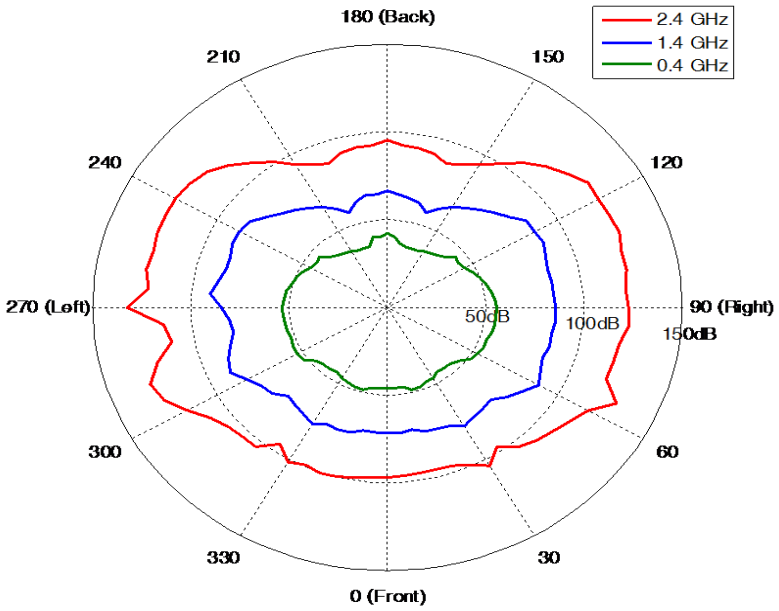

Figure 7.15: Angular dependent path loss for on body receiver.

Table 7.6: Comparison of angular dependent path loss at different frequencies.

Frequencies (GHz)	**0.4**	**1.4**	**2.4**
Average (dB)	46.316	76.74442	108.8819
Maximum difference (dB)	20.3373	33.04337	45.38211
Peak to Average Ratio	1.197665	1.171730	1.208047

7.7.3.2 Frequency Dependent Characteristics

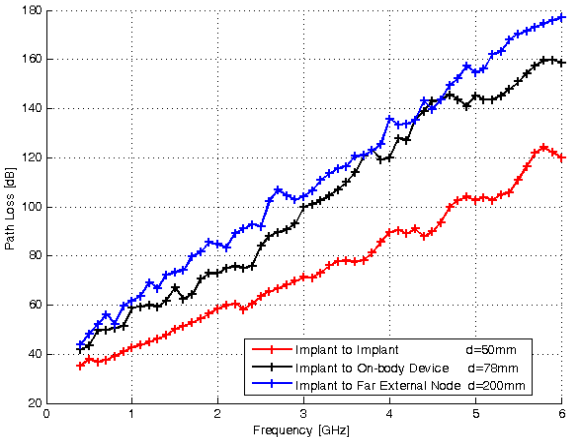

Figure 7.16: Frequency dependent path loss at different locations. ©2015 IEEE. Reprinted with permission from [55].

Since the EM waves propagate through the frequency dependent materials inside the body, the operating frequency has an important effect on the path loss model as well. The frequency dependent characteristics of the *in vivo* channel were investigated by performing simulations from 0.4 GHz to 6 GHz at 0.1 GHz increment. The *in vivo* antenna was implanted in the abdomen (78 mm in depth from the body surface) and the *ex vivo* antenna was placed at three different locations: Ὼسِ υ πάϊ ά (in body), Ὼسِ χ ψάϊ ά (on body), Ὼسِ ς π ώτά ά (far external node), where Ὼ denote the distance between the transmitter and receiver. The path loss was measured for these three scenarios (implant to implant, implant to on-body, and implant to far external node) and the results are plotted in Figure 7.16 [55]. It is observed that the frequency dependent path loss [in dB] increases linearly. Therefore, the frequency dependent *in vivo* path loss [in ratio] increases exponentially, which is faster than that in free space.

7.7.3.4 Time Dispersion Characteristics

In addition to the path loss, the time dispersion characteristics of the *in vivo* channel were investigated for different body regions using a power delay profile in the simulation environment as shown in Figure 7.17. It is observed that greater dispersion is present in the sides than anterior or posterior body locations at 915 MHz. Interestingly, the torso area exhibits an exponential decaying behavior on the dB scale while linear decaying is observed for the classical indoor/outdoor channel models [28]. The maximum excess delay is not more than 10 ns which might be negligible for narrow-band communications. However, for UWB communications, which is also a very popular signaling scheme in WBAN research, this dispersion may lead to a significant interference effect, and should be carefully considered in the waveform design.

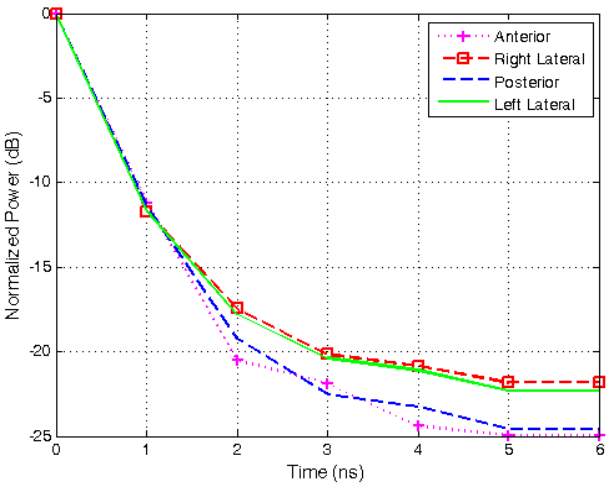

Figure 7.17: Power delay profile for each body side. ©2014 IEEE. Reprinted with permission from [45].

7.8 Comparison of *In Vivo* and *Ex Vivo* Channels

We summarize the differences between the *in vivo* and *ex vivo* channels in Table 7.7.

Table 7.7: Comparison of *in vivo* and *ex vivo* channels.

Feature	*Ex vivo*	*In vivo*
Physical Wave Propagation	Constant speed Multipath	Variable speed Multipath – plus pene
Attenuation and Path Loss	Lossless medium (losses are negligible) Path loss is essentially uniform Increases with distance	Very lossy medium Location dependent Increases exponentially with distance inside the body
Dispersion	Multipath delays - time dispersion	Multipath delays of variable speed - frequency dependent time dispersion
Near Field Communications	Deterministic near-field region around the antenna	Inhomogeneous medium - near field region changes with angles and position inside body
Power Limitations	Average and Peak	Average and Peak - Plus specific absorption rate (SAR)
Shadowing	Follows a *log-normal* distribution	Follows a *log-normal* distribution
Multipath Fading	Flat / frequency selective fading	Lower speed of propagation causes longer dispersion than in free space.
Antenna	Antenna gain is essentially location independent	"Implant location" d
Wavelength	In free space - the speed of light divided by operational frequency	$\lambda = \frac{c}{f}$ (e.g. at 2.4 GHz - roughly 6 times shorter than the wavelength in free space)

7.9 Summary

In this chapter, the state-of-the-art of *in vivo* wireless channel characterization has been presented. Various studies described in the literature are dedicated to the *in vivo* communication channel, and they consider different parameters in studying various anatomical regions. Furthermore, the location dependent characteristics of *in vivo* wireless communication at 915 MHz are analyzed in detail via numerical and experimental investigations. A complete model for the *in vivo* channel is not available and remains an open research problem. However, considering the expected future growth of implanted technologies and their potential use for the detection and diagnosis of various health related issues in the human body, the channel modeling studies should be further extended to develop better and more efficient communications systems for future *in vivo* systems.

References

[1] IEEE standard for local and metropolitan area networks: Part 15.6: Wireless body area networks," IEEE submission, Feb 2012, IEEE Std.

[2] P. S. Hall and Y. Hao, Antennas and Propagation for Body-Centric Wireless Communications. 2nd Edition, Norwood, MA: Artech House, 2012.

[3] S. Yu, X. Lin, and J. Misic, "Networking for big data [gu pp. 4–4, July 2014.

[4] A. Taparugssanagorn, A. Rabbachin, M. Hamalainen, modelling for wireless body area network in wireless medical communicatio Symp. On Wireless Personal Multimedia Communications (WPMC), 2008.

[5] A. Kiourti, K. A. Psathas, and K. S. Nikita, "I telemetry functionalities: A review of current status and cha 1–15, August 2013.

[6] S. Movassaghi, M. Abolhasan, J. Lipman, D. Smith, : A survey," Communuc s and Tutorials IEEE, vol. 16, pp. 1–29, 2014.

[7] M. R. Basar, F. Malek, K. M. Juni, M. I. Saleh, M. S. Idris, L. Mohamed, N. Saudin, and N. A. Mohd Affendi, "The use of a human body model to determi channel in wireless capsule endoscopy," Progress in Electromag – 513, 2013.

[8] T. P. Ketterl, G. E. Arrobo, A. Sahin, T. J. Tillman, H. Arslan, and R. D. Gitlin, "*In Vivo* Wireless Communication Channels," IEEE 13th Annual Wireless and Microwave Technology Conference (WAMICON), 2012.

[9] D. Smith, D. Miniutti, T. Lamahewa, A. Hanlen, -area networks: A survey and new outlook," Antennas and Propagation M – 117, Oct 2013.

[10] Q. H. Abbasi, A. Sani, A. Alomainy and Y. Hao, "On-Body Radio Channel Characterisation and System-Level Modelling for Multiband OFDM Ultra Wideband Body-Centric Wireless Network ", IEEE Transactions on Microwave Theory and Techniques, Vol. 58, no. 12, pp. 3485-3492, December 2010.

[11] Q. H. Abbasi, A. Sani, A. Alomainy and Y. Hao, "Numerical Characterisation and Modelling of Subject-Specific Ultra Wideband Body-Centric Radio Channels and Systems for Healthcare Applications", IEEE Transaction on Information and Technology In Biomedicine, Volume 16, no. 2, pp. 221-227, March 2012.

[12] S. Gabriel, R. Lau, and C. Gabriel, "The dielec the frequency range 10 hz to 20 g Physics in me p. 2251, 1996.

[13] S. Gabriel, R. W. Lau, and C. Gabriel, "The die models for the dielectric spectrum of tissues," Ph – 2293, 1996.

[14] A. Alomainy and Y. Hao, "Modeling and characterization of implants considering organ contents," Antennas and 999 –1005, April 2009.

[15] A. Pellegrini, A. Brizzi, L. Zhang, K. Ali, Y. Hao, X. Wu, C. Constantinou, Y. Nechayev, P. Hall, N. Chahat et al., "Anten-centric wireless communications at millimeter- for body wave frequencies: A review [wireless corner]," Ant no. 4, pp. 262 –287, 2013.

[16] J. Lee, S. H. annd Lee, Y. J. Yoon, S. Park, S. C antenna for ingestible capsule endoscope systems: experimental results in a human phantom and a pig," IEEE Trans. B, vol. 58, no. 6, pp. 1734 –1741, June 2011.

[17] R. Chavez-Santiago, I. Balasingham, J. Bergsland, W. Zahid, K. Takizawa, R. Miura, and H.-B. Li, "Experimental implant communication of high data r Engineering in Medicine and Biology Society (EMBC), 2013 35th Annual International Conference of the IEEE. IEEE, 2013, pp. 5175 –5178.

[18] H.-Y. Lin, M. Takahashi, K. Saito, and K. Ito, "Char different locations of the human body for in-body wireless communication," I Propag., vol. 61, pp. 5350 –5354, Oct. 2013.

[19] http://www.ansys.com/Products.

[20] A. F. Demir, Q. H. Abbasi, Z. E. Ankarali, M. Qaraqe, E. Serpedin and H. Arslan, "Short Paper: Experimental Characterization of *In Vivo* Wireless Communication Channels", in IEEE Vehicular Technology Conference (VTC), Boston, USA, 6-9 Sept. 2015.

[21] B. Latre, B. Braem, I. Moerman, C. Blondia, an networks," Wireless Networks, vol. 17, pp. 1 –18, Nov. 2010.

[22] Yazdandoost and K. Yekeh., Wireless Mobile Communication and Healthcare. Springer Berlin Heidelberg, 2012, ch. A Radio Channel Model for In-body Wireless Communications, pp. 88 –95.

[23] "C95.1-200S: IEEE Standard for Safety Levels With Respect to Human Exposure to Radio Frequency Electromagnetic Fields, 3 kHz to 300 GHz," 2006., IEEE Std.

[24] T. P. Ketterl, G. E. Arrobo, and R. D. Gitlin, “SA for *in vivo* communication at 2.4 GHz,” in Wireless and M (Wamicon), IEEE, 2013.

[25] W. Scanlon, “Analysis of tissue-coupled antennas for UHF intra-body communications,” 200

[26] M. S. Wegmueller, A. Kuhn, J. Froehlich, M. Oberle, N. Felber, N. Kuster, and W. Fi attempt to model the human body as a communicatio Transactions on, vol. 54, no. 10, pp. 1851–1857, 2007.

[27] A. T. Barth, M. A. Hanson, H. C. Powell Jr, D. Unluer, S. G. Wilson, and J. Lach, “Body-coupled communication for body sensor networks” in Proceed Body area networks. ICST (Institute for Computer Sciences, Social-Informatics and Telecommunications Engineering), 2008, p. 12.

[28] R. C.-S. Khaleghi and I. Balasingham, “Ultra-wideband statistical propagation channel model for implant sensors in the human chest,” IET Microwaves

[29] R. Chavez-Santiago, K. Sayrafian-Pour, A. Khaleghi, K. Takizawa, J. Wang, I. Balasingham, and H.-B. Li, “Propagation models for ieee 802.15.6 stan networks,” Communications Magazine, IEEE, vol. 51,

[30] K. Yang, Q. Abbasi, K. Qaraqe, A. Alomainy, and Y. Hao, “Body-centric nano-networks: em channel characterisation in water at the terahertz band,” Japan, Nov., 2-5 2014, pp. 1–5.

[31] A. Sani, A. Alomainy, and Y. Hao, “Numerical characterization and link budget evaluation of wireless implants considering different digital human phant Transactions on, vol. 57, pp. 2605–2613, Oct. 2009.

[32] K. Sayrafian-Pour, W.-B. Yang, J. Hagedorn, J. Terrill, K. Yekeh, Yazdandoost, and K. Hamaguchi, “Channel models for medical implant communication,” pp. 105–112, Dec. 2010.

[33] H. Bahrami, B. Gosselin, and L. A. Rusch, “Real of implantable wireless uwb communication systems,” Society (EMBC) Annual International Conference, IEEE, 2012.

[34] A. Johansson, “Wireless communication with med dissertation, Lund University, 2004.

[35] J. Kim and Y. Rahmat-Samii, “Implanted antennas inside a huma characterizations,” Microwave Theory and Technique 1934–1943, 2004.

[36] J. Gemio, J. Parron, and J. Soler, “Human body effects o applications: Models comparison and propagation Research, vol. 110, pp. 437–452, Oct. 2010.

[37] F. Merli, B. Fuchs, J. R. Mosig, and A. K. Skrivervik, “The effect o performance of implanted antennas,” Antennas and P pp. 21–31, 2011.

[38] K. Y. Yazdandoost and R. Kohno, “Wireless communications for medical devices,” Asia-Pacific Microwave Conference, 2007.

[39] J. R. Reitz, J. M. Frederick, and R. W. Christy, Foundations of Electromagnetic theory (4th ed.). Addison-Wesley. ISBN 0-201- 52624-7, 1993.

[40] S. H. Lee, J. Lee, Y. J. Yoon, S. Park, C. Cheon, K. Kim, and S. Nam, “A wi ingestible capsule endoscope systems: experimental Trans. Biomed. Eng., vol. 58, pp. 1734–41, Jun. 2011.

[41] T. Karacolak, A. Z. Hood, and E. Topsakal, “Design of a dual-band implantable antenna and development of skin mimicking gels for continuous Techniques, IEEE Transactions on, vol. 56, pp. 1001–1008, April 2008.

[42] A. Laskovski and M. Yuce, “A MICS telemetry implant powered by a 27MHz ism Engineering in Medicine and Biology Society,EMBC, 2011 Annual International Conference of the IEEE, 2011.

[43] A. Kiourti and K. Nikita, “Miniature scalp-implantable antennas for telemetry in the mics and ism bands: Design, safety considerations and link bud Transactions on, vol. 60, no. 8, pp. 3568–3575, Aug., 2012.

[44] M. L. Scarpello, D. Kurup, H. Rogier, D. Vande Ginste, F. Axisa, J. Vanfleteren, W. Joseph, L. Martens, and G. Vermeeren, “Design of an implanta biomedical applications,” Antennas and Propagation, –3564, 2011.

[45] A. F. Demir, Q. H. Abbasi, Z. E. Ankarali, E. Serpedin, and H. Arslan, “Nu *in vivo* wireless communication channels,” in IEEE Inter and Wireless Technologies for Biomedical and Healthcare Applications (IMWS), 2014.

[46] Z. N. Chen, G. C. Liu, and T. S. See, "Transmission of
space and implanted in the human head," Antennas a
pp. 1850–1854, 2009.
[47] L. C. Chirwa, P. Hammond, S. Roy, and D. R. S. Cumming, "Electromagnetic
sources in the human intestine between 150 MHz and 1.2 GHz," IEEE Trans. Biomed. E
pp. 484–492, Apr. 2003.
[48] S. K. S. Gupta, S. Lalwani, Y. Prakash, E. Elsharawy, and L. Schwiebert, "Towards a propagation
model for wireless biomedical applications," in IEEE Int. Conference on Communications (ICC),
2003.
[49] R. Chavez-Santiago, K. Sayrafian-Pour, A. Khaleghi, K. Takizawa, J. Wang, I. Balasingham, and H.-
B. Li, "Propagation models for IEEE 802.15.6 standardization of implant communication in body area
networks," Communications Magazine, IEEE, vol. 51,
[50] K. Y. Yazdandoost, K. Sayrafian-Pour et al., "Channel model for bod
P802, vol. 15, 2009.
[51] S. Stoa, C. S. Raul, and I. Balasingham, "An ul
human abdominal region," in GLOBECOM Workshops (GC
[52] "ANSYS HFSS®." [Online]. http://www.ansys.com/Products/Electronics/ANSYS+HFSS®. [Accessed: 12-Nov-2015].
[53] Rahman, A.; Yang Hao, "A novel tapered slot CPW-fed antenna for ultra-wideband applications and its on/off-body performance," Antenna Technology: Small and Smart Antennas Metamaterials and Applications, 2007, IWAT '07. International Workshop on , vol., no., pp.503,506, 21-23 March 2007.
[54] DeGroot, Morris H., and Mark J. Schervish. "Probability and statistics." (2002).
[55] Y. Liu and R. D. Gitlin, "A Phenomenological Path Loss Model of the *In Vivo* Wireless Channel," IEEE 16th Wireless and Microwave Technology Conference (WAMICON), April 2015.
[56] C. He, Y. Liu, G. E. Arrobo, T. P. Ketterl and R. D. Gitlin, "*In Vivo* Wireless Communications and Networking," Information Theory and Applications Workshop (ITA), 2015, San Diego, CA, February 2015.
[57] A. F. Demir, Z. E. Ankarali, Q. H. Abbasi, Y. Liu, E. Serpedin, K. Qaraqe, H. Arslan and R. D. Gitlin "State of the Art of *In Vivo* Wireless Communication Channels", accepted for publication in IEEE Vehicular Technology Magazine, 2016.